

# Doppler Boosted Dust Emission and Cosmic Infrared Background–Galaxy Cross-Correlations: A New Probe of Cosmology and Astrophysics

Abhishek S. Maniyar<sup>1,2,3,\*</sup>, Simone Ferraro<sup>4,5</sup> and Emmanuel Schaap<sup>2,3,4,5</sup>


<sup>1</sup>Center for Cosmology and Particle Physics, Department of Physics, New York University, New York, New York 10003, USA

<sup>2</sup>Kavli Institute for Particle Astrophysics and Cosmology, Stanford University, 452 Lomita Mall, Stanford, California 94305, USA

<sup>3</sup>SLAC National Accelerator Laboratory, 2575 Sand Hill Road, Menlo Park, California 94025, USA

<sup>4</sup>Lawrence Berkeley National Laboratory, One Cyclotron Road, Berkeley, California 94720, USA

<sup>5</sup>Berkeley Center for Cosmological Physics, Department of Physics, University of California, Berkeley, California 94720, USA

 (Received 20 April 2022; revised 7 October 2022; accepted 5 December 2022; published 24 January 2023)

We identify a new cosmological signal, the Doppler-boosted cosmic infrared background (DB CIB), arising from the peculiar motion of the galaxies whose thermal dust emission source the cosmic infrared background (CIB). This new observable is an independent probe of the cosmic velocity field, highly analogous to the well-known kinematic Sunyaev-Zel’dovich (KSZ) effect. Interestingly, DB CIB does not suffer from the “KSZ optical depth degeneracy,” making it immune from the complex astrophysics of galaxy formation. We forecast that the DB CIB effect is detectable in the cross-correlation of CCAT-Prime and DESI-like experiments. We show that it also acts as a new CMB foreground which can bias future KSZ cross-correlations, if not properly accounted for.

DOI: [10.1103/PhysRevLett.130.041001](https://doi.org/10.1103/PhysRevLett.130.041001)

**Introduction.**—The kinematic Sunyaev-Zel’dovich (KSZ) effect is the shift in the energy of the cosmic microwave background (CMB) photons when they undergo Thomson scattering off coherently moving electrons in the gas in galaxies, groups, and clusters [1,2]. The KSZ signal is linear in gas density and independent of the temperature of the gas. This makes it a crucial unbiased probe of these electrons on the outskirts of halos and clusters out to high redshift which are otherwise hard to detect.

Using different techniques, the KSZ signal has been successfully measured through a combination of the CMB and galaxy survey data (e.g., [3–5]). Thus, the KSZ effect is now a well-established tool to localize the “missing baryons” which reside outside the virial radius of the galaxies in an ionized, diffuse, and cold gas known as the warm-hot intergalactic medium [4]. Apart from being a tracer of this gas, the KSZ signal is also a powerful probe of the radial velocities on large scales (e.g., [6–8]). This makes the KSZ effect a probe of dark energy [9], modified gravity [10], cosmic growth rate of structure [11], primordial non-Gaussianity of local type ( $f_{\text{NL}}$ ) [12] when used in combination with other matter tracers like galaxies. These techniques, however, suffer from the well-known problem of “KSZ–optical depth degeneracy,” where the overall normalization of the electron profile in a halo is not known very well. So although we can measure the shape of the velocity power spectrum well with a combination of KSZ and galaxies, this degeneracy leads to an unknown overall normalization of the measured velocity field.

In this Letter, we present a new observable which is very analogous to the KSZ effect but does not suffer from the

“optical depth degeneracy” which KSZ suffers from. This observable is the Doppler boosted emission of the cosmic infrared background (CIB), which we will call DB CIB from here onward (Fig. 1). The CIB is cumulative infrared

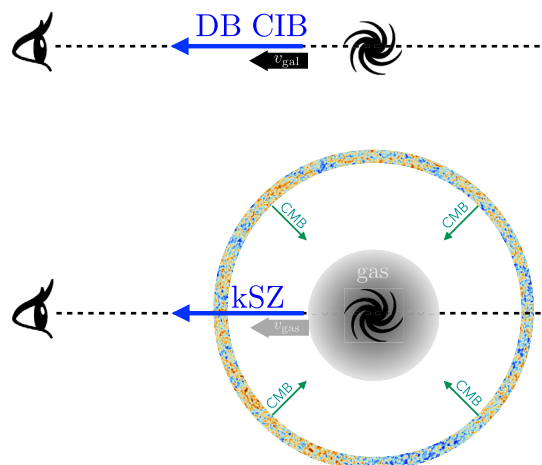


FIG. 1. Although the DB CIB effect is analogous to the KSZ, there is a subtle difference between the two. While the KSZ pertains to the Doppler effect of the CMB photons scattering off of hot intracluster gas, DB CIB is the Doppler effect on the infrared emission from a galaxy with a peculiar velocity along our line of sight. Thus, the KSZ is proportional to the optical depth of the hot gas  $\tau$ , whereas DB CIB is insensitive to it, and thus probes the velocity field without “ $\tau$  degeneracy.” In the above case, both the hot gas and galaxy are moving toward us resulting in the upshifting of the photon energy through the KSZ and DB CIB effect, respectively.

emission from all the dusty star forming galaxies throughout the Universe [13]. It is an excellent probe of the cosmic star formation and the large scale structure of the Universe [14,15].

If a galaxy contributing to the CIB has a nonzero line-of-sight peculiar velocity, its emission is Doppler boosted. The large-scale cosmic velocity field results in galaxy bulk motions, which in turn source the DB CIB signal of interest in this Letter.

Unlike KSZ, the DB CIB does not originate from scattering CMB photons: the Doppler boosting is imprinted on the galaxy’s thermal dust emission. However, the DB CIB signal is deeply analogous to the KSZ: it measures the product of velocities with the mean infrared luminosity. Crucially, this mean infrared luminosity can be measured independently, unlike the KSZ optical depth. It is thus “calibratable” and can be removed, providing unbiased estimates of the velocity field. This is precisely the reason we do not have an analogous optical depth degeneracy here. In this Letter, we compute for the first time the expected signal-to-noise ratio (SNR) for the detection of this signal for a Planck-like [16] and Fred Young submillimeter telescope (CCAT-Prime)–like [17] experiment. This effect also acts as a contaminant to the KSZ measurements from the CMB power spectrum and from the cross-correlation of CMB with galaxies. We will quantify this contamination in this Letter.

The remainder of this Letter is organized as follows. In the following section on “Doppler-boosted CIB emission,” we derive the formalism to quantify this DB CIB emission. Then, in the second part on “Cross-correlation with galaxies,” we present the formalism to detect this effect through cross-correlation of the CIB with velocity-weighted density field. We then present the expected SNR of this signal for the Planck and CCAT-Prime experiments in combination with the CMASS [18] catalog from the Baryon Oscillation Spectroscopic Survey (BOSS) and the Dark Energy Spectroscopic Instrument (DESI) galaxy survey (section on “Forecasts”). We present potential applications of this signal in the Discussion and Conclusions section.

*Doppler-boosted CIB emission.*—For any specific intensity  $I(\nu)$  at frequency  $\nu$ , the quantity  $I(\nu)/\nu^3$  is a conserved quantity under Lorentz transformations, including boosts. Using this and taking cosmological expansion into account, the fractional change in the specific intensity due to Doppler boosting is

$$\frac{\Delta I^{\text{DB}}(\nu_0)}{I(\nu_0)} = \beta(3 - \alpha_{\nu_0}) + \mathcal{O}(\beta^2), \quad (1)$$

where  $\beta = v/c \ll 1$  with  $v$  being the source peculiar velocity with respect to us and  $c$  is the speed of light,  $\nu_0$  is the observed frequency, and  $\alpha_{\nu_0}$  is the logarithmic slope of the observed intensity with respect to the observed

frequency [see Eq. (5) and Fig. 1 in Supplemental Material [19]]. A detailed derivation is presented in Supplemental Material, Sec. I [19].

This is analogous to the kinematic Sunyaev-Zeldovich (KSZ) effect (Fig. 1) where the fractional change in the CMB temperature due to the bulk flow motion of the hot gas comes out to be  $\Delta T^{\text{KSZ}}/T \propto \tau\beta$  where  $\tau$  is the optical depth of the hot gas which is not known *a priori*. Peculiar velocity field measurements using the KSZ therefore suffer from the “KSZ-optical depth degeneracy.” For the DB CIB effect on the other hand, all the terms are *calibratable*, as we shall see, and there is no such degeneracy.

Importantly, the equation so far applies to *any* emission process, including infrared emission giving rise to the CIB, but also synchrotron emission and any other radiative process across the whole electromagnetic spectrum. In what follows, we shall study the case of the CIB in detail, since the CIB dominates the extragalactic emission at millimeter and submillimeter frequencies. For the CIB,  $I^{\text{obs}}(\nu_0)$  can be calculated using Eq. (14), details of which are provided in Supplemental Material, Sec. III [19]. This requires a prior knowledge of the effective spectral energy distribution (SED)  $S_{\nu_0}^{\text{eff}}(z)$  of the infrared (IR) galaxies at a given redshift and frequency. We use the  $S_{\nu_0}^{\text{eff}}(z)$  templates from a stacking analysis presented in [23]. An alternative approach in [13] fits for  $S_{\nu_0}^{\text{eff}}(z)$  with a modified blackbody parametrization such that  $S_{\nu_0}^{\text{eff}}(z) \propto \nu_0^{\beta_d} B_{\nu_0}[T_d(z)]$  where  $B_{\nu_0}$  denotes the Planck function,  $T_d$  denotes the dust temperature as a function of redshift, and  $\beta_d$  is the emissivity index encoding information about the physical nature of the dust. In Fig. 1, we show  $\alpha_{\nu_0}$  as a function of the observed frequency and redshift for these two choices of SEDs. Looking at Eqs. (1) or (6), we see that the DB CIB emission is proportional to a factor of  $(3 - \alpha_{\nu_0})$ . We find that  $\alpha_{\nu_0} \approx 3$  for frequencies between  $\sim 100$ – $500$  GHz for different redshifts when we use SEDs from [23]. Thus, the Doppler-boosted signal might be reduced for these choices of frequencies. Interestingly, the spectral index  $\alpha_{\nu_0}$  becomes negative at high frequencies. This indicates a dropoff of intensity with respect to the observed frequency, when observing above 1.5–2.5 THz depending on the model and the redshift of the source. Since the factor of  $(3 - \alpha_{\nu_0})$  is increased for negative  $\alpha_{\nu_0}$ , the Doppler boosting of the CIB is more prominent at higher frequencies.

At very low frequencies ( $\nu < 70$  GHz) where we expect the CIB intensity to dropoff, template SEDs from [23] instead flatten out, leading to  $\alpha_{\nu_0} \approx 0$  in this case. At such low frequencies, synchrotron radiation coming from extragalactic sources compensates for the drop in the infrared emission making the final intensity almost constant with frequency which results in  $\alpha_{\nu_0} \approx 0$ . While this effect is included in the template SEDs from [23], it is not included in the modified blackbody template shown in the dashed curves and therefore the value of  $\alpha_{\nu_0}$  differs between the

two SEDs at these low frequencies. The synchrotron radiation itself is also Doppler boosted, allowing us to treat it with the same formalism.

*Cross-correlation with galaxies.*—The DB CIB signal is too small to be detected at the power spectrum level as we show in Supplemental Material, Sec. VI [19]. To detect this effect, we rely on two facts: (i) along with the KSZ, DB CIB is the only other component correlated with velocities and (ii) at high frequencies where CIB dominates and the KSZ contribution is negligible (see next section on “Forecasts”). Thus, our approach to the DB CIB detection follows the KSZ detections by [3,4], who stacked the ACT CMB maps, appropriately weighted by an external tracer of peculiar velocity, at the positions of the BOSS galaxies. Here, we propose a similar procedure through cross-correlation of the observed raw map at high frequencies (where CIB dominates) with a density-weighted velocity field (momentum)  $\mathbf{q}(\mathbf{x})$  from the galaxy positions.

In the Limber and flat sky approximations, the angular cross-power spectrum of the fluctuations in the raw high frequency map  $\Delta I(\nu_0)$  and the line of sight component of  $\mathbf{q}(\mathbf{x})$  i.e.,  $q_\gamma(\mathbf{x})$  is

$$C_\ell^{\Delta I_{\nu_0}^{\text{DB}} q_\gamma} = \int \frac{d\chi}{\chi^2} W^{\Delta I_{\nu_0}}(\nu_0, z) W^q(z) P^{\Delta I_{\nu_0} q_\gamma} \left( \frac{\ell + 1/2}{\chi}, z \right), \quad (2)$$

where  $\chi$  is the comoving distance to redshift  $z$ ,  $W^{\Delta I_{\nu_0}}(\nu_0, z)$  and  $W^q(z)$  are the window functions corresponding to the CIB fluctuations and the galaxy survey, respectively.  $P^{\Delta I_{\nu_0} q_\gamma} \{[(\ell + 1/2)/\chi], z\}$  is the cross-power spectrum of the fluctuations in the raw map and the line-of-sight component  $q_\gamma$  which is given as

$$P^{\Delta I_{\nu_0} q_\gamma}(k, z) = (3 - \alpha_{\nu_0}) P^{\Delta I_{\nu_0} \delta_g}(k, z) \langle \beta_{\text{LOS}}^2 \rangle(z), \quad (3)$$

where  $\langle \beta_{\text{LOS}}^2 \rangle(z)$  is the variance of the line of sight velocity and  $P^{\Delta I_{\nu_0} \delta_g}(k, z)$  is the cross-power spectrum of the CIB fluctuations and the galaxy overdensity field. A detailed derivation is provided in Supplemental Material, Sec. II [19].

Equation (3), together with Eq. (2) and the approximation in Eq. (9) (Supplemental Material, Sec. II [19]) represent the main result of this Letter. The last ingredient needed to evaluate the expected signal is the cross-correlation between CIB fluctuations and galaxies,  $P^{\Delta I_{\nu_0} \delta_g}(k, z)$ . We calculate this cross power spectrum following the CIB halo model from [21] and the details are provided in Supplemental Material, Sec. III [19]. From Eq. (3), we can see that three points which make DB CIB nonzero and detectable in cross-correlation with the momentum field are the following: nonzero velocities of galaxies ( $\beta \neq 0$ ), the correlation between the galaxies in our spectroscopic catalog and the galaxies which emit the CIB ( $P^{\Delta I_{\nu_0} \delta_g}$ ),

and the frequency-dependence of the CIB, which avoids  $\alpha_{\nu_0} = 3$ .

*Forecasts.*—Here, we present the signal-to-noise ratio (SNR) for the cross-correlation of the raw frequency map with the momentum field. While  $C_\ell^{\Delta I_{\nu_0}^{\text{DB}} q_\gamma}$  is the signal we are after, the noise includes all the components in the raw frequency map. In practice however, at the high frequencies we consider, the CIB and detector noise dominate. As a result, the SNR is calculated as

$$\left( \frac{S}{N} \right)^2 = f_{\text{sky}} \sum_{\ell_{\text{bmin}}}^{\ell_{\text{bmax}}} \frac{(2\ell_b + 1) \Delta \ell (C_{\ell_b}^{\Delta I_{\nu_0}^{\text{DB}} q_\gamma})^2}{(C_{\ell_b}^{\Delta I_{\nu_0}^{\text{DB}} q_\gamma})^2 + C_{\ell_b}^{\Delta I_{\nu_0} \Delta I_{\nu_0}} \times C_{\ell_b}^{q_\gamma q_\gamma}}, \quad (4)$$

where

$$C_{\ell_b} = \frac{1}{\Delta \ell} \sum_{\ell \in [\ell_1, \ell_2]} C_\ell, \quad (5)$$

and  $\Delta \ell$  is the bin width.

$C_{\ell_b}^{\Delta I_{\nu_0} \Delta I_{\nu_0}}$  is the total binned CIB auto power spectrum at frequency  $\nu_0$ , i.e., it is the sum of the one-halo, two-halo, and the shot-noise power spectra,  $C_{\ell_b}^{\Delta I_{\nu_0} \Delta I_{\nu_0}} = C_{\ell_b, 1h}^{\Delta I_{\nu_0} \Delta I_{\nu_0}} + C_{\ell_b, 2h}^{\Delta I_{\nu_0} \Delta I_{\nu_0}} + C_{\ell_b, \text{shot}}^{\Delta I_{\nu_0} \Delta I_{\nu_0}}$ . We also add a detector white-noise term  $N_\ell^{\text{det}}$  to this for various experiments described below.  $C_{\ell_b}^{q_\gamma q_\gamma}$  is the galaxy radial velocity field power spectrum. It is obtained from  $P^{q_\gamma q_\gamma}(k, z) = P^{\delta_g \delta_g}(k, z) \langle \beta_{\text{LOS}}^2 \rangle(z)$ , following Eq. (3).

As previously mentioned, we use a halo model approach to calculate all the auto- and cross-power spectra, with full details in Supplemental Material, Sec. III [19]. Similar to the case of the CIB, for the galaxy auto- and CIB  $\times$  galaxy cross-power spectra, we sum up the 1-halo, 2-halo, and shot noise power spectrum contributions. For the CIB  $\times$  galaxy power spectra, we estimate the cross-shot noise term for a given frequency as

$$C_{\ell_b, \text{shot}}^{\Delta I_{\nu_0} \delta_g} = \sqrt{C_{\ell_b, \text{shot}}^{\Delta I_{\nu_0} \Delta I_{\nu_0}} \times C_{\ell_b, \text{shot}}^{\delta_g \delta_g}}. \quad (6)$$

In practice, this is an upper limit to the cross-shot noise term, as it assumes that the shot noise of CIB and galaxies are perfectly correlated. Since the actual level of cross-shot noise is uncertain, we only include it when forecasting the CIB SNR, not the DB CIB SNR. Perhaps counterintuitively, this choice is actually conservative, and can only lead to underestimating the DB CIB SNR. Indeed, the cross-shot noise is both part of our signal and noise (via its cosmic variance), but the noise contribution is negligible, since we are far from cosmic variance limited. Formally, this can be seen from Eq. (4), where the cross-shot noise term appears both in the numerator and the denominator. However, in the denominator, the cross-power spectrum is

TABLE I. Experimental specifications used in this Letter. Planck and CCAT-Prime specifications are taken from [16] and [17]. The detector noise is quoted in thermodynamic differential CMB temperature units.

Experiment	$\ell_{\min}$	$\ell_{\max}$	$\Delta_T$ $\mu\text{K-arcmin}$	$\sigma$ $\text{arcmin}$
Planck (545 GHz)	100	5000	1137.0	4.7
Planck (857 GHz)	100	5000	29075.0	4.3
CCAT-prime (410 GHz)	100	50 000	372.0	0.5
CCAT-prime (850 GHz)	100	50 000	$5.7 \times 10^5$	0.2

small compared to the product of the auto spectra, in our noise dominated regime. As a result, including the cross-shot noise would have no effect on the noise, but would enhance the signal. This enhanced signal will mostly be seen on very small scales ( $\ell \gtrsim 3000$ ).

For the CIB part, we assume two different setups which correspond to Planck-like and CCAT-Prime-like experiments. For the galaxy survey, we assume four different galaxy samples corresponding to the CMASS-like ( $0.44 < z < 0.70$ ), DESI ELG-like ( $0.0 < z < 2.0$ ), DESI LRG-like ( $0.0 < z < 1.4$ ), and extended DESI ELG-like ( $0.0 < z < 4.0$  and denoted as Ext. DESI ELG) galaxy samples. Ext. DESI ELG is assumed to be a hypothetical galaxy survey which detects the same number of galaxies as DESI ELG survey, but extended over twice the redshift range. To calculate the galaxy and CIB  $\times$  galaxy power spectra within a halo model framework, a halo occupation distribution (HOD) is required. Here, we use the HOD corresponding to the CMASS survey developed by [34]. We use the same HOD parametrization for the DESI ELG, DESI LRG, and Ext. DESI ELG samples as well with a minor tweak: we adjust the minimum galaxy mass detectable for different samples such that the total numbers of galaxies detected by these surveys match the expected numbers from these surveys. While not exact, this should be a reasonable approximation for our purposes. The sky fraction is assumed to be  $f_{\text{sky}} = 0.4$ .

Our assumed experimental setups which correspond to the Planck-like and CCAT-Prime-like experiments are given in Table I. The Gaussian random noise of the detector is calculated as

$$N_{\ell}^{\text{det}} = (\Delta_T)^2 e^{\ell(\ell+1)\sigma^2/8\ln 2}, \quad (7)$$

where  $\Delta_T$  denotes the white noise of the detector in  $\mu\text{K-arcmin}$  or  $\text{Jy/sr}$ , and  $\sigma$  is the full width at half maximum (FWHM) of the beam in radians. As shown in [15,35], galactic dust dominates over the CIB power spectra below  $\ell \sim 100$ , and therefore we choose  $\ell_{\min} = 100$  in Table I.

Figure 2 shows  $C_{\ell}^{\Delta I_{\nu_0}^{\text{DB}} q_T}$  for a CCAT-Prime-like 850 GHz map and DESI ELG-like map with error bars. Our predictions for the expected SNR on the  $C_{\ell}^{\Delta I_{\nu_0}^{\text{DB}} q_T}$  for the

TABLE II. SNR for  $C_{\ell}^{\Delta I_{\nu_0}^{\text{DB}} q_T}$  different different configurations considered here. For CCAT-Prime-like experiment considered here, in the third column we assume shot noise to be equal to shot noise from Planck for corresponding frequency, while in the fourth column shot noise for CCAT-Prime is 10 times smaller than Planck. Unbracketed and bracketed numbers show SNR at 545 and 857 GHz, respectively for Planck, and at 410 and 850 GHz, respectively for CCAT-Prime.

	Galaxy exp	DB CIB SNR	
		High shot	Low shot
Planck	CMASS	0.05 (0.37)	
545 (857)	DESI ELG	0.98 (5.03)	
GHz	DESI LRG	0.35 (3.66)	
	Ext. DESI ELG	1.75 (5.67)	
CCAT-Prime	CMASS	0.01 (2.30)	0.01 (2.35)
410 (850)	DESI ELG	3.71 (51.77)	4.36 (52.82)
GHz	DESI LRG	1.96 (31.27)	2.32 (31.93)
	Ext. DESI ELG	15.21 (68.42)	18.00 (69.85)

experimental specifications considered here are given in Table II. Forecasts for  $C_{\ell}^{\Delta I_{\nu_0}^{\text{DB}} \delta_g}$  are presented in Table I in Supplemental Material, Sec. III [19]. As an in-depth study of the flux-cut limits for CCAT-Prime is beyond the scope of this Letter, we consider two limiting cases: (i) shot noise for CCAT-Prime is equal to the shot-noise for Planck and (ii) CCAT-Prime has 10 times lower shot noise than Planck. While the third column in Tables I and II corresponds to case (i), the fourth column corresponds to case (ii) for CCAT-Prime experiment.

As can be seen from these tables,  $C_{\ell}^{\Delta I_{\nu_0}^{\text{DB}} \delta_g}$  can be detected to very high SNR. On the other hand, the DB CIB signal  $C_{\ell}^{\Delta I_{\nu_0}^{\text{DB}} q_T}$  detection will be challenging with a Planck-like experiment considered here. A combination of CCAT-Prime and DESI surveys should be able to detect  $C_{\ell}^{\Delta I_{\nu_0}^{\text{DB}} q_T}$  with a high ( $> 5$ ) SNR for 850 GHz channel.

The CMASS, DESI, and Ext. DESI surveys considered here trace galaxies around redshifts  $\sim 0.5$ ,  $\sim 1.0$ , and  $\sim 2.0$ , respectively. Therefore, SNR for  $C_{\ell}^{\Delta I_{\nu_0}^{\text{DB}} \delta_g}$  for Planck is higher with 857 GHz channel than 545 GHz channel as for the CIB higher frequencies trace relatively lower redshifts and vice versa (e.g., [14]). However, this is not the case for CCAT-Prime experiment where SNR is lower for 850 GHz than 410 GHz. This is mainly due to the significant higher instrumental noise at 850 GHz than 410 GHz. The logic applied here has to be slightly modified while looking at Table II for SNR on  $C_{\ell}^{\Delta I_{\nu_0}^{\text{DB}} q_T}$ . As we can see from Eq. (12), calculation of  $C_{\ell}^{\Delta I_{\nu_0}^{\text{DB}} q_T}$  from  $C_{\ell}^{\Delta I_{\nu_0}^{\text{DB}} \delta_g}$  involves extra factors of  $(3 - \alpha_{\nu_0})$  and  $\langle \beta_{\text{LOS}}^2 \rangle(z)$  which depend on frequency and redshift, respectively. The factor of  $(3 - \alpha_{\nu_0})$  is smaller at 545 (410) GHz than at 857 (850) GHz (Fig. 1).

Also, for the redshifts considered here,  $\langle \beta_{\text{LOS}}^2 \rangle(z)$  decrease with increasing redshifts. Combining these two things again with the fact that CIB at higher frequencies traces galaxies at lower redshifts, we can see that SNR for  $C_\ell^{\Delta I_{\nu_0} \delta_g}$  and  $C_\ell^{\Delta I_{\nu_0}^{\text{DB}} q_r}$  is higher at 857 (or 850) GHz than at 545 (or 410) GHz for Planck (or CCAT-Prime) experiment considered here. We note that in this calculation we use the actual redshift range corresponding to our galaxy samples to calculate  $\alpha_{\nu_0}$  unlike what we show in Fig. 1, where  $\alpha_{\nu_0}$  is calculated after integrating the CIB emission between  $0 < z < z_s$  for different source redshifts  $z_s$ .

For the extended DESI ELG like survey considered here, we see that both  $C_\ell^{\Delta I_{\nu_0} \delta_g}$  and  $C_\ell^{\Delta I_{\nu_0}^{\text{DB}} q_r}$  are detected at higher SNR than other surveys. In the case of  $C_\ell^{\Delta I_{\nu_0} \delta_g}$  this is solely due to obtaining the signal over a larger range of redshift (thus larger overlap with CIB redshifts [14]) compared to other surveys. As can be seen from Fig. 1, the value of  $\alpha_{\nu_0}$  is lower when galaxies over a broad redshift range (e.g., Ext. DESI ELG:  $0 < z < 4$ ) are considered compared to a narrower range (e.g. DESI ELG:  $0 < z < 2$ ). This results in a higher value of the  $(3 - \alpha_{\nu_0})$  factor which enters in the calculation of  $C_\ell^{\Delta I_{\nu_0}^{\text{DB}} q_r}$  for surveys of broader redshift range. Combined with the larger redshift overlap with the CIB, this effect adds to have higher SNR for  $C_\ell^{\Delta I_{\nu_0}^{\text{DB}} q_r}$  detection with Ext. DESI ELG survey compared to other surveys.

The SNR in case (ii) for CCAT-Prime experiment in Table I is smaller than in case (i) which has a higher shot noise compared to former. This is because the cross-shot noise term given in Eq. (6), adds to the signal for CIB  $\times$  galaxy cross-correlation. This is not the case for  $C_\ell^{\Delta I_{\nu_0}^{\text{DB}} q_r}$  where there is no cross-shot noise term in Eq. (4) and only the autoshot power spectrum for the CIB and galaxy survey appear in the denominator acting as noise decreasing the SNR. Therefore, unlike for CIB  $\times$  galaxy, the SNR slightly increases for case (ii) compared to case (i). In other words, unlike for the case of CMB observations where decreasing foreground levels by masking sources is beneficial, in our case the Doppler-boosted emission from the sources is our signal, and therefore aggressive masking is not guaranteed to lead to higher SNR. In fact, more aggressive masking will reduce the noise (by reducing shot noise), but will also reduce the signal. A full study of the optimal flux cuts that maximize the SNR is beyond the scope of this Letter.

*Discussion and conclusions.*—Emission coming from the CIB galaxies gets boosted by the Doppler effect as a result of their motion in the large scale cosmological velocity field. In this Letter, we present a formalism to calculate this effect and quantify the detectability of the cross-correlation of the CIB with a velocity weighted galaxy density field. We show that although this effect

would be hard to detect through a cross-correlation of Planck and CMASS/DESI galaxies, a combination of the CCAT-Prime and DESI survey can potentially detect this signal.

We show that the KSZ effect acts as a bias to the DB CIB measurement and vice versa, i.e., the DB CIB constitutes a new source of foreground while measuring the KSZ power spectrum, and a bias to stacking-based KSZ estimators (Supplemental Material, Secs. IV–VI [19]). For upcoming CMB experiments like SO and CMB-S4 which plan to detect the KSZ at a very high significance, this foreground contamination will have to be considered and removed. We point out in Supplemental Material, Sec. V [19], this can be done using the distinct frequency dependence, as well as the different angular profile of this effect.

As mentioned in the Introduction, the radial velocity field is an excellent cosmological probe. It has been shown that the KSZ tomography technique can be successfully used to measure the radial velocity field with the upcoming CMB surveys [8,12]. Because of the “KSZ optical depth degeneracy,” the overall normalization of the measured velocity is not known *a priori* and must be marginalized over. This is not an issue for measurements of  $f_{\text{NL}}$  due to the scale dependence of the signal, but it poses a significant challenge for measurements that require knowledge of the normalization, such as growth of structure which depend on the amplitude of the velocity power spectrum.

From Eq. (3), we can see that the DB CIB emission can act as a new observable to reconstruct the velocity field  $\beta$ , free from this degeneracy. Thus, we can construct an estimator for  $\beta$  using a combination of a CIB and galaxy survey or solely using the CIB. This estimator has an advantage over the KSZ tomography technique as it does not suffer from the “optical depth degeneracy” as the intensity of the CIB emission at a given frequency  $I_\nu$  is *calibratable* by direct measurement of the cross-correlation  $C_\ell^{\Delta I_{\nu_0} \delta_g}$  (or by stacking). As can be seen from Table I, the SNR on  $C_\ell^{\Delta I_{\nu_0} \delta_g}$  is always a lot greater the SNR of the DB CIB signal, so that the uncertainty on the calibration is always subdominant and should not limit the inference of the velocity field.

Thus, the velocities detected through such a technique will be a useful cosmological probe. In fact, it has to be noted that such an effect of Doppler boosting is not limited to the CIB emitting galaxies and is generalizable to any galaxy population. Therefore, such a formulation can be used with the galaxies detected through the powerful upcoming surveys like DESI, Euclid, and Roman Space Telescope. In an upcoming Letter, we will present such an estimator of velocity and its predictions for cosmological constraints.

We thank Neal Dalal, Jacques Delabrouille, Colin Hill, Anthony Pullen, and David Spergel for useful

conversations. S. F. is supported by the Physics Division of Lawrence Berkeley National Laboratory. E. S. was supported by the Chamberlain fellowship at Lawrence Berkeley National Laboratory, and is now supported by the Kavli Institute for Particle Astrophysics and Cosmology at SLAC National Accelerator Laboratory.

\*amaniyar@stanford.edu

- [1] R. A. Sunyaev and Y. B. Zeldovich, *Comments Astrophys. Space Phys.* **4**, 173 (1972).
- [2] R. A. Sunyaev and Y. B. Zeldovich, *Mon. Not. R. Astron. Soc.* **190**, 413 (1980).
- [3] E. Schaan *et al.*, *Phys. Rev. D* **93**, 082002 (2016).
- [4] E. Schaan (Atacama Cosmology Telescope Collaboration), *Phys. Rev. D* **103**, 063513 (2021).
- [5] A. Kusiak, B. Bolliet, S. Ferraro, J. C. Hill, and A. Krolewski, *Phys. Rev. D* **104**, 043518 (2021).
- [6] P. Zhang, *Mon. Not. R. Astron. Soc.* **407**, L36 (2010).
- [7] A.-S. Deutsch, E. Dimastrogiovanni, M. C. Johnson, M. Münchmeyer, and A. Terrana, *Phys. Rev. D* **98**, 123501 (2018).
- [8] K. M. Smith *et al.*, [arXiv:1810.13423](https://arxiv.org/abs/1810.13423).
- [9] S. DeDeo, D. N. Spergel, and H. Trac (2005).
- [10] E.-M. Mueller, F. de Bernardis, R. Bean, and M. D. Niemack, *Astrophys. J.* **808**, 47 (2015).
- [11] D. Alonso, T. Louis, P. Bull, and P. G. Ferreira, *Phys. Rev. D* **94**, 043522 (2016).
- [12] M. Münchmeyer, M. S. Madhavacheril, S. Ferraro, M. C. Johnson, and K. M. Smith, *Phys. Rev. D* **100**, 083508 (2019).
- [13] Planck Collaboration *et al.*, *Astron. Astrophys.* **571**, A30 (2014).
- [14] A. S. Maniyar, M. Béthermin, and G. Lagache, *Astron. Astrophys.* **614**, A39 (2018).
- [15] A. Maniyar, G. Lagache, M. Béthermin, and S. Ilić, *Astron. Astrophys.* **621**, A32 (2019).
- [16] Planck Collaboration *et al.*, *Astron. Astrophys.* **571**, A6 (2014).
- [17] S. K. Choi *et al.*, *J. Low Temp. Phys.* **199**, 1089 (2020).
- [18] C. P. Ahn *et al.*, *Astrophys. J. Suppl. Ser.* **211**, 17 (2014).
- [19] See Supplemental Material at <http://link.aps.org/supplemental/10.1103/PhysRevLett.130.041001> for detailed derivation, which includes Refs. [3–4,13,20–33].
- [20] C.-P. Ma and J. N. Fry, *Phys. Rev. Lett.* **88**, 211301 (2002).
- [21] A. Maniyar, M. Béthermin, and G. Lagache, *Astron. Astrophys.* **645**, A40 (2021).
- [22] J. Tinker, A. V. Kravtsov, A. Klypin, K. Abazajian, M. Warren, G. Yepes, S. Gottlöber, and D. E. Holz, *Astrophys. J.* **688**, 709 (2008).
- [23] M. Béthermin *et al.*, *Astron. Astrophys.* **573**, A113 (2015).
- [24] J. L. Tinker and A. R. Wetzel, *Astrophys. J.* **719**, 88 (2010).
- [25] J. L. Tinker, B. E. Robertson, A. V. Kravtsov, A. Klypin, M. S. Warren, G. Yepes, and S. Gottlöber, *Astrophys. J.* **724**, 878 (2010).
- [26] A. Cooray and R. Sheth, *Phys. Rep.* **372**, 1 (2002).
- [27] S. Ferraro, J. Colin Hill, N. Battaglia, J. Liu, and D. N. Spergel, *Phys. Rev. D* **94**, 123526 (2016).
- [28] J. C. Hill, S. Ferraro, N. Battaglia, J. Liu, and D. N. Spergel, *Phys. Rev. Lett.* **117**, 051301 (2016).
- [29] N. Battaglia, S. Ferraro, E. Schaan, and D. Spergel, *J. Cosmol. Astropart. Phys.* **11** (2017) 040.
- [30] P. Ade *et al.*, *J. Cosmol. Astropart. Phys.* **02** (2019) 056.
- [31] K. Abazajian *et al.* (2019).
- [32] L. D. Shaw, D. H. Rudd, and D. Nagai, *Astrophys. J.* **756**, 15 (2012).
- [33] F. McCarthy and M. S. Madhavacheril, *Phys. Rev. D* **103**, 103515 (2021).
- [34] S. More, H. Miyatake, R. Mandelbaum, M. Takada, D. N. Spergel, J. R. Brownstein, and D. P. Schneider, *Astrophys. J.* **806**, 2 (2015).
- [35] D. Lenz, O. Doré, and G. Lagache, *Astrophys. J.* **883**, 75 (2019).